Theor. Comput. Fluid Dyn.
DOI 10.1007/s00162-011-0251-9

ORIGINAL ARTICLE

Patricio Bohorquez · Luis Parras

Three-dimensional numerical simulation of the wake flow of an afterbody at subsonic speeds

Received: 14 April 2011 / Accepted: 9 December 2011

Abstract We numerically investigate the wake flow of an afterbody at low Reynolds number in the incompressible and compressible regimes. We found that, with increasing Reynolds number, the initially stable and axisymmetric base flow undergoes a first stationary bifurcation which breaks the axisymmetry and develops two parallel steady counter-rotating vortices. The critical Reynolds number (Re_{cs}) for the loss of the flow axisymmetry reported here is in excellent agreement with previous axisymmetric BiGlobal linear stability (BiGLS) results. As the Reynolds number increases above a second threshold, Re_{co}, we report a second instability defined as a three-dimensional peristaltic oscillation which modulates the vortices, similar to the sphere wake, sharing many points in common with long-wavelength symmetric Crow instability. Both the critical Reynolds number for the onset of oscillation, Re_{co}, and the Strouhal number of the time-periodic limit cycle, St_{sat}, are substantially shifted with respect to previous axisymmetric BiGLS predictions neglecting the first bifurcation. For slightly larger Reynolds numbers, the wake oscillations are stronger and vortices are shed close to the afterbody base. In the compressible regime, no fundamental changes are observed in the bifurcation process. It is shown that the steady state planar-symmetric solution is almost equal to the incompressible case and that the break of planar symmetry in the vortex shedding regime is retarded due to compressibility effects. Finally, we report the developments of a low frequency which depends on the afterbody aspect ratio, as well as on the Reynolds and on the Mach number, prior to the loss of the planar symmetry of the wake.

Keywords Bluff body · Hydrodynamic stability · Laminar wake · Vortex instability · OpenFOAM

1 Introduction

The study of external flows over afterbodies has attracted the interest of engineers and physicists during the last decades because of its practical relevance [36]. Most authors focused their attention on the characterisation of aerodynamics variables in flight conditions, i.e., for compressible flows at transonic/supersonic speeds and turbulent regime. However, the analysis of the instability mechanisms developing in laminar regime as the

Communicated by Colonius.

Electronic supplementary material The online version of this article (doi:10.1007/s00162-011-0251-9) contains supplementary material, which is available to authorized users.

P. Bohorquez (✉)
Área de Mecánica de Fluidos, Departamento de Ingeniería Mecánica y Minera,
Universidad de Jaén, Campus de las Lagunillas, 23071 Jaén, Spain
E-mail: patricio.bohorquez@ujaen.es

L. Parras
E. T. S. Ingenieros Industriales, Universidad de Málaga, Dr. Ortiz Ramos s/n, 29071 Málaga, Spain

Published online: 30 December 2011

Reynolds number increases, which may lead to turbulence, is an outstanding problem which remains still unresolved.

The present work is hence motivated by a wish to accurately characterise the bifurcation process and the ensuing saturated non-linear regimes in the laminar wake of a slender afterbody at subsonic speeds, as well as to discuss its relation with the incompressible case. Such aim has been considered recently for subsonic flows by means of axisymmetric BiGlobal linear stability (BiGLS) analysis [16,17], showing that the initially stable and axisymmetric base flow undergoes a series of bifurcations with increasing Reynolds number: the first bifurcation is stationary and breaks the axisymmetry, whereas the second one is oscillatory and leads to the onset of periodic flow oscillations. Such bifurcation scenario is analogous to that of the sphere in the incompressible regime, which has been object of experiments [11,21,25], axisymmetric BiGLS [9,20,22], direct numerical simulations (DNS) [9,12,33,34] and TriGlobal linear stability (TriGLS) analyses [19,30,37].

In the case of the incompressible wake flow of a sphere, it is now well understood that axisymmetric BiGLS deals properly with the first regular bifurcation, which occurs according to experiments and DNS at $Re_{cs} \approx 210$. Furthermore, the shift of the critical oscillatory Reynolds number predicted by axisymmetric BiGLS, 277.5 [20], is small with respect to the consensual threshold for the onset of vortex shedding, 272 [9], and the refined experimental value obtained recently by Gumowski et al. [11], who found out a three-dimensional peristaltic instability at $Re_{co} \approx 267$. To the authors' knowledge, the peristaltic instability was reported just from the experimental side [11,25], though the kink in the steady trailing vortex filaments was earlier quantified in the numerical simulations by Thompson et al. [33], who speculated that the kinking increment in the range of Re between Re_{cs} and Re_{co} could be associated with the transition to the periodic state. Furthermore, though Gumowski et al. [11] mentioned that the peristaltic instability is reminiscent of Crow instability [5,7,14,24], the vortex filament properties were not quantified (in particular, the vortices centres, circulation and radius). Morzyński and Thiele [19] and Theofilis [31] have recently pointed out that TriGLS would be formally needed in order to better understand the second oscillatory bifurcation, defined as a three-dimensional peristaltic instability prior to the onset of vortex shedding [11]. However, in order to analyse TriGLS properties of the oscillatory mode, one requires filtered solutions of the Navier–Stokes equations to get the unstable base flow and new generation algorithms to formulate and to solve for the eigenvalue problem, needing a large amount of time and computational resources. The complexity of such analysis can be understood in view of TriGLS results for the oscillatory mode of the laminar wake of a sphere, which are nowadays scarce and limited to the specific parameter values of $Re = 300$ for $M = 0$ [19] and $M = 0.6$ [37].

Indeed, TriGlobal permits a reduction to a sequence of axisymmetric and nonaxisymmetric BiGLS, see Sect. 3.5 in [31], but the results described in the literature for the wake flow of an afterbody only cover the first axisymmetric BiGLS analysis, and larger discrepancies appear for this type of geometry in the BiGLS prediction of Re_{co} with respect to experiments and DNS [2]. To overcome this limitation three-dimensional temporal simulations are performed here in the incompressible and compressible regimes. It is already known that DNS is consistent with axisymmetric BiGLS at determining the critical parameters associated with the loss of the flow axisymmetry in the wake flow of a sphere [31]. In addition, we have shown that DNS values of Re_{cs} and Re_{co} accurately match BiGlobal and experimental results, respectively, for the laminar incompressible wake of a short blunt-based axisymmetric body [2]. In compressible regime, a good agreement has also been found between GLS and DNS under several scenarios, e.g. [4]. In addition, DNS provides the Strouhal number St_{sat}, associated with the (nonlinear) frequency of the time-periodic limit cycle, for Reynolds numbers above Re_{co}. It is worth mentioning that the (linear) frequency given by a global stability analysis does not necessarily match the non-linear frequency as the Reynolds number progressively increases far from Re_{co}, as happens, for instance, in the case of a circular cylinder [1,13,27]. Therefore, the authors believe that DNS by itself is a valuable tool to quantify the critical parameters close to the steady and oscillatory neutral curves and that results reported herein may serve to motivate a more involved global linear stability in the configuration under study here. As a matter of fact, we shall show for the first time that the peristaltic instability is analogous to long-wavelength symmetric Crow instability with the vortex filaments moving on planes inclined about 35° to the horizontal.

So, this article is aimed at reviewing and extending the bifurcations in the wake flow of an afterbody of high aspect ratio at moderate Reynolds number ($Re \leq 1{,}000$) in the incompressible ($M = 0$) and compressible ($M = 0.5$) regimes. We start with the formulation of the problem in Sect. 2. Next in Sect. 3, we present some numerical simulations and draw out the connections between this analysis and the previous ones, showing the applicability of our numerical findings. The incompressible and compressible planar-symmetric base flows in the range of Reynolds numbers $Re_{cs} < Re < Re_{co}$ are described in detail in Sects. 3.1.1 and 3.2.1, respectively. We shall put a particular focus on the oscillatory bifurcation for incompressible flows (Sect. 3.1.2). The main

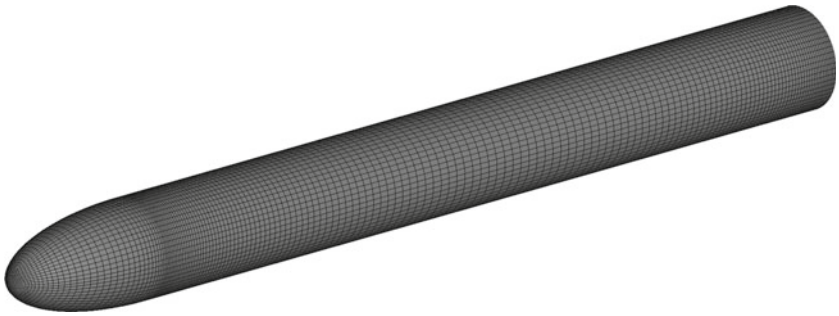

Fig. 1 Front view of the afterbody mesh

new features are that three-dimensional effects originating from the loss of the background flow axisymmetry and the growth of the pair of trailing vortices are taken into account. The oscillatory regime and the excitation of non-linear frequencies in incompressible flows and at subsonic speeds for $Re_{\rm co} < Re \leq 1{,}000$ are subsequently described in Sects. 3.1.3 and 3.2.2, respectively. Finally, we draw some conclusions.

2 Formulation of the problem

For the sake of comparison, we analysed the same geometry employed in previous axisymmetric BiGlobal linear stability studies [16,17], see Fig. 1. The cylindrical body diameter is D, and its total length is $L = 9.8\,D$, with an ellipsoidal rounded nose of 3:1 major-to-minor axis ratio, aligned with the direction of the free stream. We solved for the compressible Navier–Stokes equations by means of a collocated finite volume method (FVM) in Cartesian coordinates and in conservative form [10]. The use of FVM, the strong conservation form of the compressible Navier–Stokes equations, and the fixed direction coordinate system ensures conservation of physical properties at the discrete level [8]. The density ρ, velocity $\mathbf{u}$, temperature T and pressure p fields were made dimensionless using the far field quantities ρ_∞, U_∞, T_∞ and p_∞ as density, velocity, temperature and pressure scales, respectively, whilst the positional vector $\mathbf{x} \equiv (x, y, z)$ was made dimensionless using D as length scale. We considered only a calorically perfect gas with ratio of specific heats at constant pressure and volume of $\gamma = c_p/c_v = 1.4$, and a unit Prandtl number [16,17]. Subsequently, the non-dimensional numbers governing the fluid dynamics are the Reynolds $Re = \rho_\infty D U_\infty/\mu$ and Mach $M = U_\infty/\sqrt{\gamma R_g T_\infty}$ numbers, where μ and R_g denote the dynamic viscosity and the ideal gas constant, respectively. We focused attention on incompressible ($M = 0$, Sect. 3.1) and compressible ($M = 0.5$, Sect. 3.2) flows.

The computational domain consists of the solid afterbody aligned with the x-axis into a coaxial external cylinder of radius $15D$ and length $125D$. The origin of the coordinate system is located at the centre of the blunt solid base of the body and the outlet of the external cylinder is located $100D$ downstream from the base of the afterbody. These upstream and radial computational lengths are similar to those employed in [2], whilst the length downstream the afterbody base was increased from $50D$ to $100D$ in order to achieve accurate results. It is worth mentioning that the downstream length of our computational domain is even larger than the low velocity water channel of $54D$ employed in [11] and that employed in the previous numerical studies of the flow around a sphere [9,12,34] of 25–30 D. As a matter of fact, we shall see in Sect. 3 that locating the outlet at $x = 100$ allows us to observe for the first time the peristaltic instability that occurs far away from the afterbody base, where the wake becomes near-parallel along the streamwise direction, and to discuss its relation with Crow's stability theory for a pair of trailing vortices [7]. That is, the use of a lower downstream length may impair the quality of the numerical results for Reynolds numbers close to the oscillatory. We imposed a far field boundary condition at the inlet of the external cylinder ($x = -25$) for a uniform fluid stream of velocity U_∞, temperature T_∞ and pressure p_∞, no-slip and adiabatic boundary conditions on the solid walls of the body, slip condition at external cylindrical surface ($y^2 + z^2 = 15^2$), and non-reflective boundary condition for the outflow ($x = 100$) [6,29]. In these conditions, the transient three-dimensional numerical simulations presented in the next section preserved the steady state even in the presence of the steady state (SS) mode without the developments of false resonance modes [29].

Parallel computations were made within 12 or 16 blocks of mesh with a total mesh of 5×10^6 hexahedras, approximately, and GNU GPL software [10]. The grid points located in the generatrix of the afterbody and along the x-axis were distributed as follows: 38 and 136 cell edges in the rounded nose and in the cylindrical generatrix, respectively (see Fig. 1); 78 and 650 cell edges in the x-axis, upstream of the rounded nose and

Table 1 Recirculation length L_r as a function of M and the critical Reynolds numbers (Re_{cs}^{GLS} and Re_{co}^{GLS}): results by an anonymous referee (private communication), denoted by AR, and our computations with a second-order accurate van Leer (VL) and first-order accurate upwind (UPW) limiter in space

M	Re_{cs}^{GLS}	Re_{co}^{GLS}	$L_r(Re_{cs}^{GLS})$		$L_r(Re_{co}^{GLS})$		
			AR	VL	AR	VL	UPW
0.0	460.50	909.10	1.824	1.818	2.251	2.235	2.018
0.1	461.34	911.69	1.829	1.821	2.254	2.238	2.020
0.3	470.10	939.02	1.867	1.843	2.310	2.270	2.071
0.5	488.40	998.56	1.951	1.943	2.432	2.386	2.165

at the back of the afterbody, respectively. The radial direction was divided into 38 ($y^2 + z^2 \leq 0.5^2$) and 78 ($y^2 + z^2 \geq 0.5^2$) edges. When distributing the grid points we ensured that the grid size is enough to solve the viscous boundary layer near the solid walls. Finally, we split the azimuthal direction into 64 sections. We refer the reader to [2] for additional details on the mesh topology. All the computations reported in this paper were performed on two clusters, where each node has eight Intel Itanium Montvale dual-core processors (Finisterrae, Centro de Supercomputación de Galicia, CESGA) and two Intel Nehalem x5670 six-core processors (Centro Informatico Científico de Andalucía, CICA). The full system of non-linear equations was solved following a segregated approach [8]. To ensure the convergence of the numerical solution at each time step, we set the number of outer loops to 4. So the residual of each conservation equation lay below 10^{-6} during the transient numerical simulations. The physical time required for computing one single outer loop was about 20 s (CESGA) and 10 s (CICA), and subsequently of 80 s (CESGA) and 40 s (CICA) for each time step. The time step was adjusted during the numerical simulation so that the Courant number [8] was lower than 0.5. Close to criticality, the runtime of a complete numerical simulation depends mainly on the growth rate of the unstable mode (i.e. on the proximity to the neutral curve): the lower growth rate, the longer the runtime required. On the other hand, the runtime corresponding to Reynolds numbers moderately larger than the oscillatory threshold depends on the excitation of new frequencies in the wake (see Sects. 3.1.2, 3.1.3): the higher the Reynolds number, the longer the runtime required. In absolute terms, the time required for each three-dimensional numerical simulation in Sect. 3 varies between one and four months.

We checked the performance of the numerical solver by comparing the recirculation length L_r with previous known numerical results at the critical Reynolds numbers for the onset of the SS mode (Re_{cs}^{GLS}) and vortex shedding (Re_{co}^{GLS}), provided an axisymmetric base flow. To this end, we used the axisymmetric version of the numerical solver. Previous results were reported by Meliga [15] employing a Finite Element Method (FEM) and refined values were given by an anonymous referee, denoted hereafter as AR (private communication). Table 1 shows the evolution of the critical Reynolds numbers obtained by means of BiGLS and the recirculation length L_r as a function of M. We also provide the values obtained in our axisymmetric computations by using two different discretisation schemes in space: a standard first-order upwind (UPW) scheme, and a second-order total-variation-diminishing and symmetric limiter, named van Leer (VL). As expected, the recirculation length L_r is underpredicted when using a standard first-order upwind scheme in space. Conversely, the numerical solution is much more accurate when we elected a second-order total-variation-diminishing and symmetric limiter. Indeed, our VL results are nearly identical to those by AR (private communication) and Meliga [15]. Therefore, we employed the second-order total-variation-diminishing scheme in the direct numerical simulations presented below. Taking into account that the accuracy of the FEM used in [15–17] is comparable to our FVM, we expect a good agreement between previous BiGLS results and our DNS for the primary instability (see Sects. 3.1.1, 3.2.1).

3 Results

3.1 Incompressible regime, $M = 0$

3.1.1 Primary instability: loss of the flow axisymmetry

In order to gain some inroads into the problem, transient three-dimensional numerical simulations were performed in the incompressible limit ($M = 0$) increasing progressively the Reynolds number. We started from the Reynolds number of $Re = 450$ that lies slightly below the critical value for the loss of the flow axisymmetry of $Re_{cs}^{GLS} = 460.5$ [15]. After a transient stage, the numerical solution reached an axisymmetric steady state at late time. We verified it during the numerical simulation by examining the temporal evolution

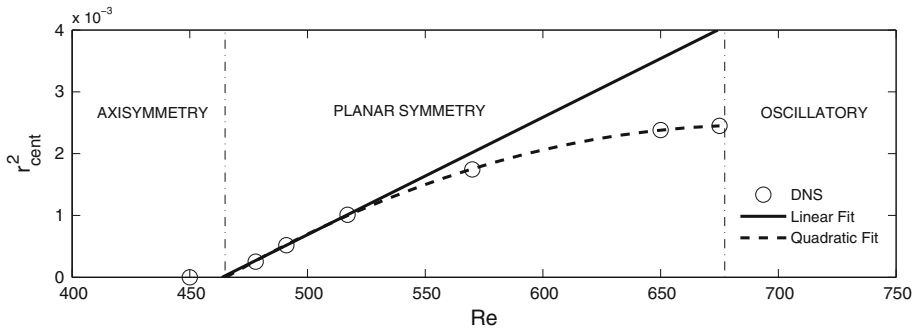

Fig. 2 Squared centroid eccentricity versus the Reynolds number at $z = 1$ (*circles*), together with a linear (*solid line*) and quadratic (*dashed line*) fit. Results for incompressible flow, $M = 0$

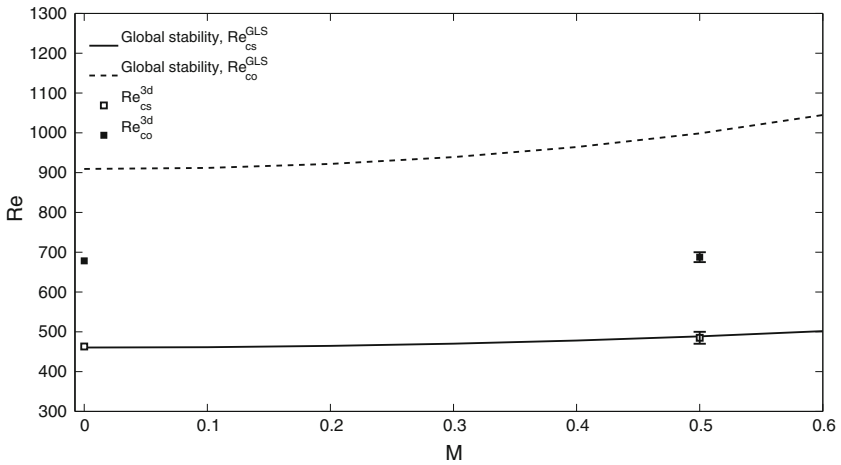

Fig. 3 Dependence of the critical Reynolds numbers on M: *continuous* and *dashed lines* depict axisymmetric GLS results [15–17] for the onset of the SS mode ($Re^{\mathrm{GLS}}_{\mathrm{cs}}$) and vortex shedding ($Re^{\mathrm{GLS}}_{\mathrm{co}}$), respectively, and *open square* and *filled square* display the values of $Re^{\mathrm{3d}}_{\mathrm{co}}$ and $Re^{\mathrm{3d}}_{\mathrm{cs}}$ determined in the present work. At $M = 0.5$ we also show the *error bar*

of the three velocity components in the cross section $x = 3$ and along five straight lines (in particular, along $\{y = 0, z = 0\}$, $\{y = 0, z = \pm 0.5\}$ and $\{y = \pm 0.5, z = 0\}$). Additional computations were performed for $Re = 478, 491, 517, 570, 650$ and 675 that reached the planar-symmetric steady state described below.

As in [2], the squared eccentricity of the vorticity contours, r^2_{cent}, was computed as a function of Re to calculate the critical Reynolds number corresponding to the first steady bifurcation from the DNS, $Re^{\mathrm{3d}}_{\mathrm{cs}}$, see Fig. 2. Close to criticality, the squared eccentricity increased linearly, and thus $Re^{\mathrm{3d}}_{\mathrm{cs}}$ was obtained by linear regression to yield $Re^{\mathrm{3d}}_{\mathrm{cs}} = 463$. This result is in accordance with the BiGLS analysis [15], see Fig. 3, which predicted the loss of the flow axisymmetry for $Re > Re^{\mathrm{GLS}}_{\mathrm{cs}} = 460.5$. Notice that the relative error between $Re^{\mathrm{3d}}_{\mathrm{cs}}$ and $Re^{\mathrm{GLS}}_{\mathrm{cs}}$ is just of 0.5%, showing that the current FVM is as accurate as the FEM employed by Meliga et al. [16,17]. Below $Re^{\mathrm{3d}}_{\mathrm{cs}}$, the eccentricity vanished because the afterbody wake was indeed axisymmetric. Conversely, the squared eccentricity increased linearly with the Reynolds number in the range of $Re^{\mathrm{3d}}_{\mathrm{cs}} < Re < 517$ and deviated from the linear dependence for larger Reynolds numbers. We found that the squared eccentricity monotonously increases without saturation up to the second oscillatory bifurcation which occurs at $Re^{\mathrm{3d}}_{\mathrm{co}} = 678.2$ (see Sect. 3.1.2). The cause of the wake eccentricity is the development of the SS mode owing the loss of the flow axisymmetry, and the growth of a well-known pair of steady streamwise counter-rotating vortices, as shown in Fig. 4, which induced a velocity at the centreline of each other and caused a misalignment with the symmetry plane. The ensuing flow field is analogous to the wake flow behind a sphere at $210 < Re < 272$ [9,11,19,21,22,25,30,33,34], does not longer exhibit a closed recirculation bubble and diverges from the unrealistic axisymmetric solution as Re increases above Re_{cs}. Due to the global nature of the instability, the developing azimuthal velocity perturbs not only the region downstream from the afterbody base but also the upstream flow, modifying the axisymmetric boundary layer. Indeed, the length of the streamwise vorticity contours $\omega_x = \pm 0.05$ is larger for $Re = 650$ (Fig. 4b) than for $Re = 478$ (Fig. 4a)

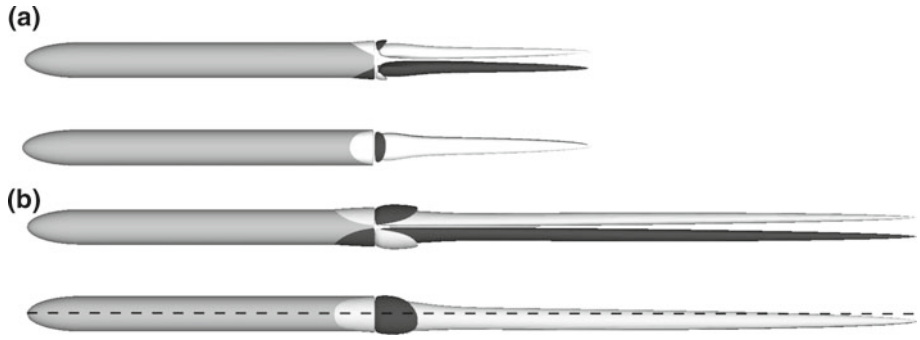

Fig. 4 Contours of constant streamwise vorticity, $\omega_x = \pm 0.05$, at $M = 0$ for the steady planar-symmetric wake at $Re = 478$ (**a**) and 650 (**b**). Plan view is rotated 90° with respect to the lateral view for each Re. The eccentricity of the vorticity contours shown in Fig. 2 at $Re = 650$ is readily illustrated in subplot **b** where the *dashed line* is the axis

Fig. 5 As Fig. 4 for $M = 0$ and $\omega_x = \pm 0.01$ at $Re = 650$ (**a**), $Re = 679$ (**b**) and $Re = 680$ (**c**). Snapshots in subplot **b** clearly illustrate the 3D peristaltic instability described for the sphere wake by Gumowski et al. [11], whilst **c** depicts the shedding of vortices in the far wake of the solid body. See movies 1 and 2 included as supplementary material to observe the oscillatory behaviour of the afterbody wake in the absence of vortex shedding at $Re = 679$

both down- and up-stream from the base. As happens in the sphere wake [11,25,33], there is a kink in the trailing vortex filaments downstream from the base, see Fig. 4a, and the vortices get closer at, approximately, 2 diameters downstream from the afterbody base for a wide range of Re (see the discussion about Crow instability in Sect. 3.1.2). The vortices get closer and closer as the Reynolds number increases similar to the sphere wake (see Figure 8 in [33]). However, a difference between the afterbody and the sphere wake is the relative gap between the critical Reynolds numbers $\Delta \equiv (Re^{3d}_{co} - Re^{3d}_{cs})/Re^{3d}_{cs}$. In particular, we get $\Delta = 0.46$ for the afterbody which is higher than for a sphere ($\Delta = 0.27$). As a consequence, the new background flow that develops prior to the development of the second oscillatory bifurcation deviates more from the axisymmetric flow in the afterbody case than for shorter solids. Indeed, Fig. 4 clearly shows the growth of the streamwise vorticity from $Re = 478$ to $Re = 650$ and, as a consequence, the developments of larger azimuthal velocities as the Reynolds number increases. Given that the first bifurcation makes the flow nonaxisymmetric and that the planar-symmetric base flow diverges from the fictitious axisymmetric solution with increasing values of Re above Re_{cs}, there is no reason to expect that the approach followed by Meliga et al. [16] should predict adequately the secondary instability, as we show below.

3.1.2 Secondary bifurcation: vortex shedding via peristaltic oscillation

An exhaustive study was performed with an eye to observe if, as for the sphere wake [11], the second instability can be defined as a 3D peristaltic oscillation which modulates the two counter-rotating vortices. To this end, we increased the Reynolds number up to $Re = 679$ and inspected the temporal evolution of the velocity field in several points of the computational domain as for the numerical simulations in Sect. 3.1.1. Once the initial transient was washed out, the velocity signal was found monochromatic at late time, with constant amplitude at each probe. So the flow reached the periodic state illustrated in Fig. 5b. The sinuously kink of the contours of constant streamwise vorticity $\omega_x = \pm 0.01$ at $Re = 679$ is evident in Fig. 5b as we move downstream from the

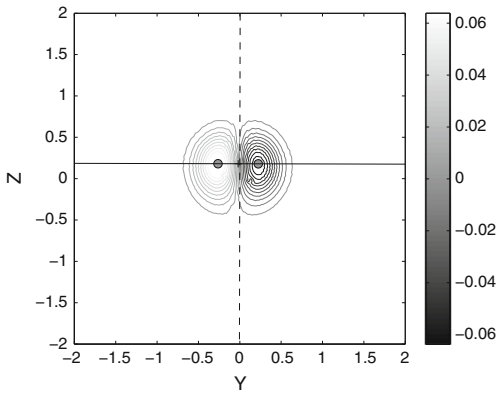

Fig. 6 Streamwise vorticity ω_x at $x = 10$ as for Fig. 5a, $Re = 650$ and $M = 0$

afterbody base and is absent in the steady planar-symmetric wake below $Re_{\text{co}}^{\text{3d}}$, as shown in Fig. 5a at $Re = 650$. Notice the absence of vortex shedding in Fig. 5b as well as in the supplementary animations 1–2. In addition, supplementary videos 3–4 show the oscillatory contours of constant streamwise vorticity $\omega_x = \pm 0.05$ that are similar to the steady ones below $Re_{\text{co}}^{\text{3d}} = 678.2$, see Fig. 4, though they exhibit a cyclical modulation which first enlarges and later decreases their length far from the afterbody base. However, the oscillation of the vortex core vanishes close to the solid base. This result is in agreement with experimental observations in [11], because the first modulations were perceptible in the far wake of the solid object and the amplitude of the oscillations grew with the downstream distance. Furthermore, by increasing slightly the Reynolds number up to $Re = 680$, we found out the shedding of vortices in the far wake when the flow reached the saturated periodic state at late time (see Fig. 5c). The shedding of vortices in the far wake of the afterbody is consistent with TriGLS results by Morzyński and Thiele [19] for the incompressible wake behind a sphere at Reynolds number slightly supercritical. Indeed, they reported vanishing amplitudes of the eigenmode at the back of the sphere and growing amplitudes further downstream. To the authors' knowledge, this is the first time that the 3D peristaltic oscillation is reported by DNS in the wake flow of a solid body and might be due to the argument advanced in Sect. 2. Previous DNS of the flow around spheres [9,12,34] and bullet shaped geometries [2] employed the downstream length of the computational domain of 25–30 D and 50 D, respectively, which are lower than that of the low velocity water channel by Gumowski et al. [11] (54 D) and the present work (100 D). Therefore, the use of a short downstream length may impair the quality of the numerical results for Reynolds numbers close to the oscillatory because the peristaltic instability occurs in the far wake.

One of the advantages of DNS is the possibility of having the flow field for all the variables in different axial locations. This allows us to further understand the physical origin of this peristaltic oscillation. Here we want to discuss its relation with Crow instability [7] as it was pointed out by Gumowski et al. [11]. We analysed the pair of counter-rotating vortices generated by the afterbody wake at different axial locations. Firstly, we get the centre of each vortex, denoted by $\mathbf{x}_\pm$. Then we calculated the distance between both vortices $b \equiv ||\mathbf{x}_+ - \mathbf{x}_-||$, and defined the region of positive and negative vorticity by the perpendicular to the line joining $\mathbf{x}_+$ and $\mathbf{x}_-$. This operation is illustrated in Fig. 6. Subsequently, we obtained the circulation of each vortex ($\Gamma_\pm$) and the second moment of the axial vorticity field, which let us define the characteristic radius a of each vortex (the positive and negative vortices in the regions defined above), as was done in [5],

$$\Gamma_\pm = \int_{S_\pm} \omega_x \, \mathrm{d}S_\pm, \quad \Gamma_\pm \, a_\pm^2 = \int_{S_\pm} \omega_x \, ||\mathbf{x} - \mathbf{x}_\pm||^2 \, \mathrm{d}S_\pm, \tag{1}$$

where S_+ and S_- correspond with the regions having positive and negative axial vorticity, respectively. By computing $a_\pm$, b and $\Gamma_\pm$ for $Re = 478$, 517, 570 and 650, we corroborated the expected result $a_+ = a_- = a$ and $\Gamma_+ = -\Gamma_- = \Gamma_o$, as shown in Fig. 7 for $0 < x \leq 80$. Notice that, independent of Re, the ratio a/b tends to the asymptotic value of 1.27 for increasing values of x, whilst Γ_o monotonously decreases with x. Interestingly, the variations of Γ_o with x are smoother for $x > 30$, indicating that the base flow is nearly parallel far enough from the body. The effect of viscosity on the spreading of the vortices must have an effect on the instability properties, as the viscosity spreads the vortices with the streamwise distance making them more stable. This fact led us to think that the peristaltic instability observed at $Re = 679$ in the far wake, see Fig. 5b, is indeed caused because of the destabilization of the pair of trailing vortices at some critical streamwise location.

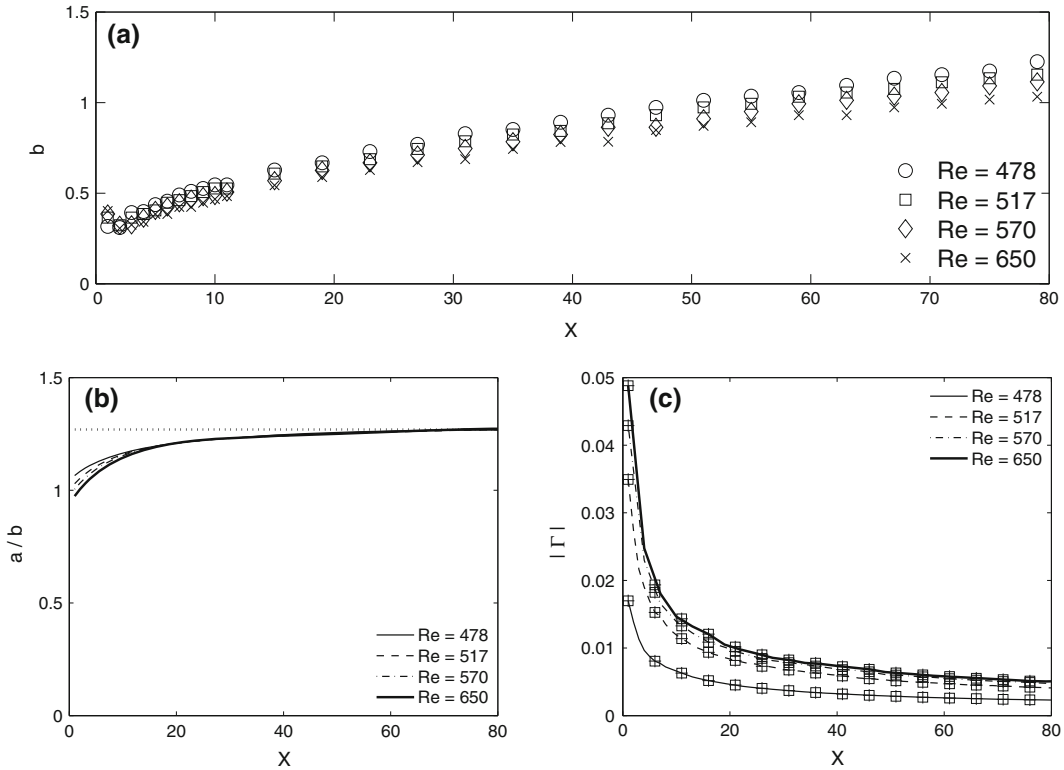

Fig. 7 **a** Distance between the vortex cores $b = ||\mathbf{x}_+ - \mathbf{x}_-||$, **b** ratio between the characteristic length of the vortex a and the distance between the vortex cores b, and **c** non-dimensional circulation of each core versus the non-dimensional axial distance to the afterbody base. *Dotted line* in **b** depicts the asymptote $a/b = 1.27$. *Plus symbol* and *squares* in **c** show the results for the vortices with negative and positive axial vorticity, respectively. Note that in **c** both symbols almost collapse. Results for incompressible flow, $M = 0$

The stability properties of a pair of counter-rotating vortices is a subject widely studied because it is a configuration that appears in the wake of aeroplanes. For a pair of counter-rotating vortices without axial core flow it is already known that the problem presents two kind of inviscid instabilities, see [14,24] and references therein: long-wavelength waves, related to the mutual induction of both vortices, referred hereafter to as Crow instability [7], and short wavelength instabilities which are related to the elliptical deformation of the core because of the presence of the other vortex, also known as Widnall (or elliptical) instability (see [18,35]). The peristaltic oscillation shown in this problem is a long-wavelength wave (several vortex cores of size). Crow instability theory is formally valid for values of $a/b \ll 1$, i.e. when both vortices are away one from the other, and is applicable for high Reynolds numbers. However, we have seen in Fig. 7b that a/b is of the order of unity in the present case at all Reynolds numbers. Indeed, the asymptote $a/b = 1.27$ shows that the results are almost invariant for $x > 25$, where the circulation Γ_o varies very slowly along the streamwise coordinate, see Fig. 7c, prior to the onset of oscillations. At Reynolds numbers slightly lower than the oscillatory threshold, we observed that Γ_o is of the order $O(10^{-2})$ for $x > 25$ and takes nearly the same values within the range $570 < Re < 650$. The corresponding vortex Reynolds number $Re_\Gamma \equiv \Gamma_o Re$ [14], based on the vortex circulation Γ_o, is of the order unity. Even in this case in which Crow instability theory is not applicable (because it is inviscid), we expect that a similar instability mechanism develops in the current case though the maximum growth rate would be highly reduced because of viscous effects. Symmetric Crow instability (mode S) consists on two displacement modes acting over each of the vortex, moving their centres in two planes inclined at about $\theta = 45°$ to the horizontal [7]. For $Re = 679$, we analysed the position of the vortex centres during several cycles, see Fig. 8, and found out that they lie on two planes forming an angle of 110° corresponding with mode S. Therefore, both vortices displace on planes inclined about $\theta = 35°$ to the horizontal. Surprisingly, the angle between planes is close to that of 104°–115° found by Roy et al [24] in experiments carried out for higher vortex Reynolds numbers in the presence of axial core flow. It is worth to note that the amplitude of the oscillation monotonously increases as a function of the streamwise distance, see Fig. 8, as usually happens for spatial amplifying waves. This is not necessarily true if the streamwise distance

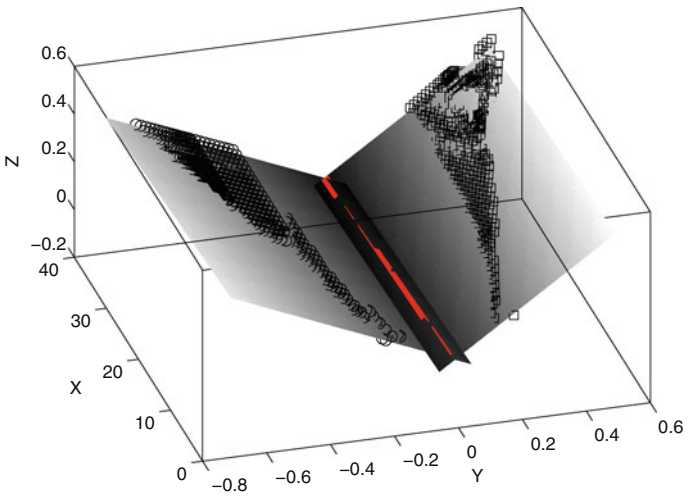

Fig. 8 Position of the positive (*circles*) and negative (*squares*) vortex centres for $M = 0$ and $Re = 679$, as for Fig. 5b, during several cycles. The best fit planes containing such points are also shown, illustrating the similarity between the peristaltic and Crow instability. The angle between planes is of 110°, and the *solid line* highlights their intersection

is increased further, as the viscosity spreads the vortices making them more stable. Subsequently, we computed the axial wavelength of the highest amplitude mode as the distance between two sequential troughs at a fixed instant of time, which yield $\lambda = 8$ for $0 < x \leq 60$, though the oscillatory modulation of the core paths was indistinguishable for $x < 15$. Taking into account that the main distance between the cores b varies along the streamwise coordinate, see Fig. 7a, the scaled non-dimensional wavelength λ/b decreases downstream from about 20 ($x = 0$) to 8 ($x = 60$). Curiously, long-wavelength instabilities reported by Leweke and Williamson lie in the same range of λ/b, see Figure 7 in [14]. To mathematically prove that this instability is associated with the destabilization of the pair of trailing vortices with axial core flow [24], similar to Crow instability but for low Reynolds numbers, a parallel BiGLS can be done at different axial locations for Reynolds number close to the oscillatory threshold. This will provide an estimation of the most unstable mode, the angle θ of the plane where the instability develops and the most dangerous axial wavelength. However, such task is outside the scope of the present work.

Finally, we observed the periodical shed of vortices close to the base by setting $Re = 685$, see Fig. 9a, and that the oscillatory bifurcation, which involved the destabilization of the steady three-dimensional branch, preserved planar (or reflectional) symmetry. Samples were also recorded at the same control points as for previous runs, showing at late time the monochromatic signal with constant amplitude in Fig. 10a, b. The non-dimensional value of t in the abscissa of Fig. 10a, c and e, was reinitialized so that the final periodic state is given by $t > 0$. The saturated amplitude of the streamwise velocity perturbation was, approximately, two orders of magnitude larger than for $Re = 679$. This is consistent with previous evidences that the vortex shedding state is a continuation of the 3D peristaltic modulation and a result of larger oscillations in the wake [11].

It is already known that the transition to the oscillatory regime corresponds to a supercritical (or nonhysteretic) Hopf bifurcation in which the squared amplitude of the velocity fluctuations increases linearly with the Reynolds number, e.g. [2,21,33]. Because the current interval of Reynolds numbers which encloses $Re_{\mathrm{co}}^{\mathrm{3d}}$ is really narrow, i.e. $650 \leq Re \leq 685$, and the non-linear saturation due to the excitation of new frequencies in the wake (i.e. the harmonics of the main frequency and low-frequency modulation) does not occur approximately at least up to $Re > Re_{\mathrm{co}}^{\mathrm{3d}} + 60$ [2], the three-dimensional global linear stability should work properly at these Reynolds numbers. Indeed, by using the periodic flow at $Re = 685$ as initial condition and decreasing the Reynolds number down to 650, we observed the exponential decay of the velocity fluctuation amplitude. In particular, we fitted the perturbation amplitude with an exponential function of time to compute the growth decay and, by interpolating it with the growth rate obtained during the simulation for $Re = 685$, we were able to find the critical value of Reynolds number for the onset of oscillations, $Re_{\mathrm{co}}^{\mathrm{3d}} = 678.2$. To the authors' knowledge, this technique was firstly applied by Ghidersa and Dušek [9] in the context of the sphere wake. We employed the same procedure to determine the oscillatory transition in the wake of a blunt-based axisymmetric body of length-to-diameter aspect ratio of 1 and 2, reporting a discrepancy lower than 5% between the DNS and the experimental critical values, and larger than 25% between axisymmetric BiGLS and DNS [2]. Similarly, the actual $Re_{\mathrm{co}}^{\mathrm{3d}} = 678.2$ is much lower than the threshold arising from axisymmetric BiGLS analyses [16,17],

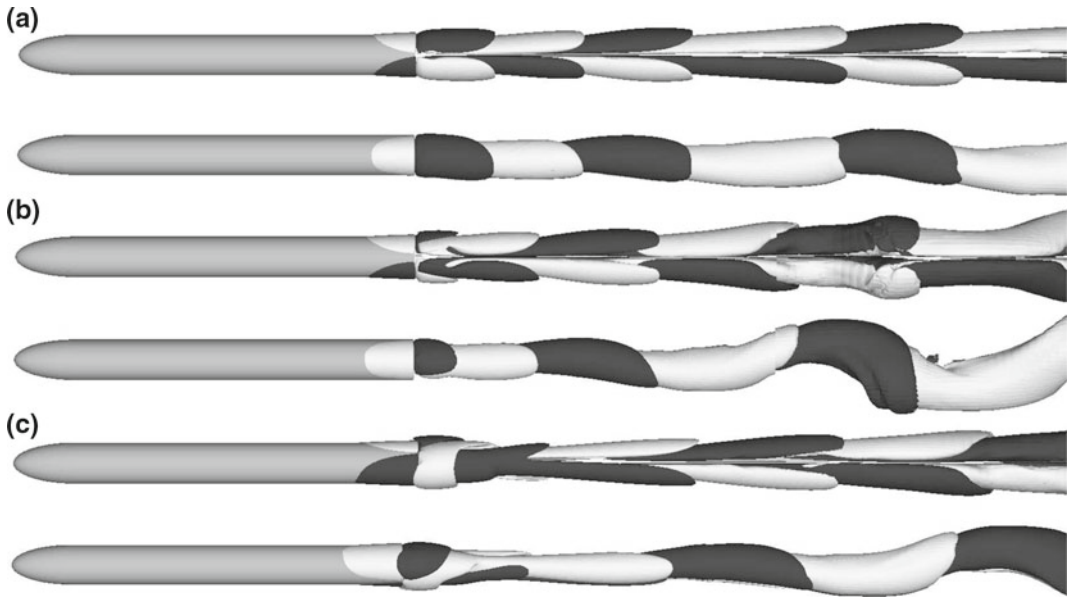

Fig. 9 Contours of constant streamwise vorticity, $\omega_x = \pm 0.05$, at $M = 0$ for $Re = 685$ (**a**), 900 (**b**) and 1,000 (**c**). Plan view is rotated 90° with respect to the lateral view

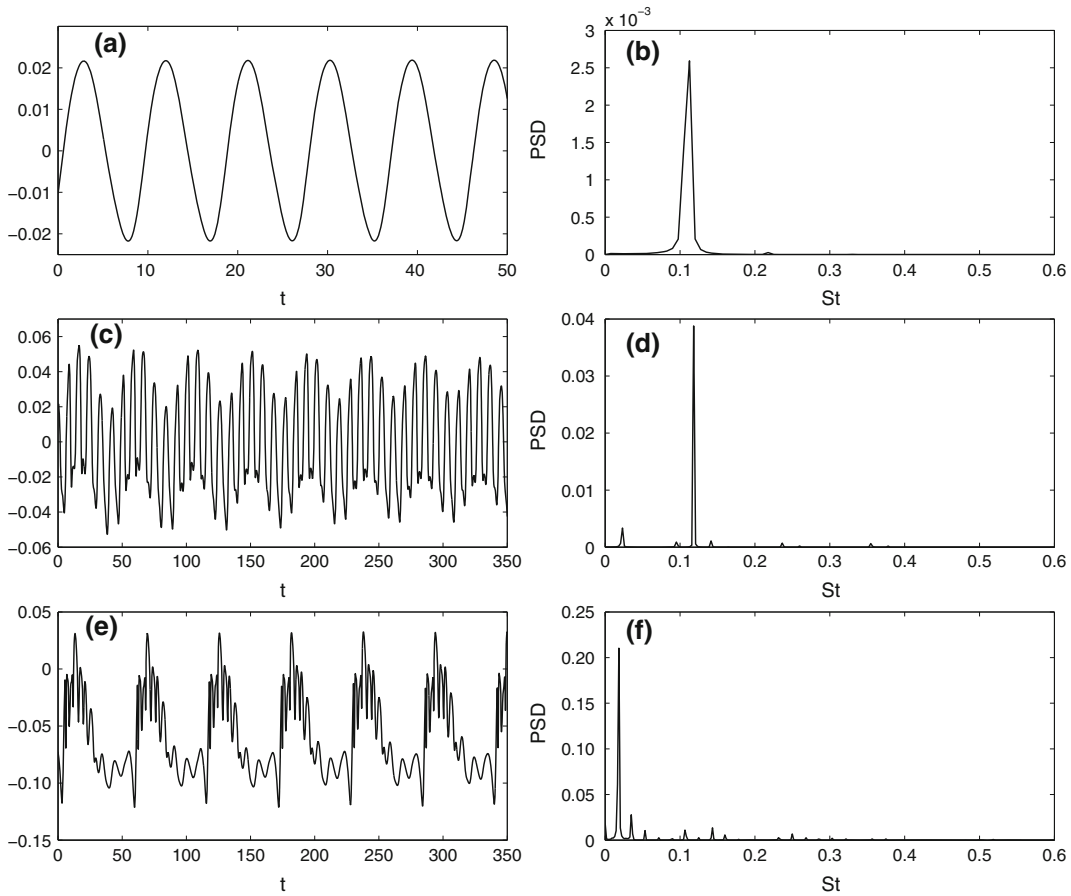

Fig. 10 Time history (*left column*) and PSD (*right column*) of the fluctuations of the streamwise velocity component [2] at $M = 0$ for **a**, **b** $Re = 685$, **c**, **d** $Re = 800$ and **e**, **f** $Re = 900$. The nondimensional value of t in the abscissa of **a**, **c** and **e** was reinitialized to show just the saturated periodic state ($t > 0$). All probes were sampled at ($x = 3$, $y = 0$, $z = 0$)

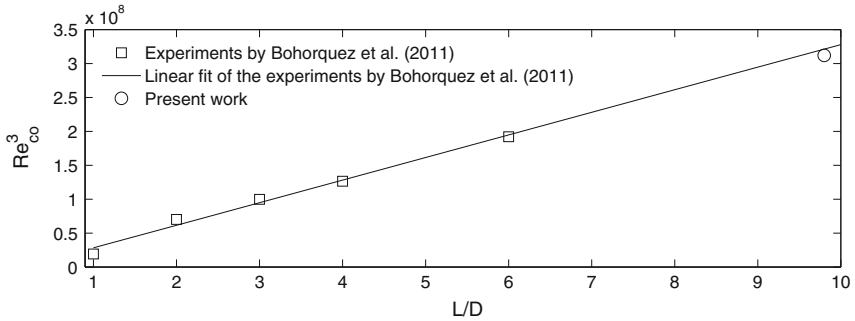

Fig. 11 Cube of the critical oscillatory Reynolds number, Re^3_{co}, as a function of the afterbody aspect ratio L/D: *squares* represent the experimental results for $1 \leq L/D \leq 6$ in Figures 13(a) and 14 from [2], and the *solid line* is their linear fit. The error between the present computations for $L/D = 9.8$ (*circle*) and the extrapolated value from experiments is lower than 1%

$Re^{GLS}_{co} = 909.1$, which leads to the discrepancy of 34%, whilst the agreement with the extrapolated value from the experiments in [2] is really good, i.e. lower than 1% (see Fig. 11). The Strouhal number of the time-periodic limit cycle at onset $St^{3d}_{sat} = 0.113$, which was obtained by computing the power spectral density (PSD) of the streamwise velocity component near criticality (see Fig. 10a, b), lies very close to the experimental (0.1294) and numerical (0.1246) value of a blunt-based axisymmetric body with a length-to-diameter ratio of 2 [2]. However, the axisymmetric BiGLS frequency [15–17], $St^{GLS}_{sat} = 0.066$, differs from the true value of St^{3d}_{sat}. So the critical values of Re^{GLS}_{co} and St^{GLS}_{sat} reported in [16] do not predict adequately the secondary instability given that the primary bifurcation makes the flow nonaxisymmetric and that the planar-symmetric base flow diverges from the fictitious axisymmetric solution at Re_{co} ($\gg Re_{cs}$), as anticipated in Sect. 3.1.1. It is worth recalling that Re^{GLS}_{co} and St^{GLS}_{sat} are the values obtained from a global stability analysis of the axisymmetric base flow, whilst Re^{3d}_{co} and St^{3d}_{sat} are the exact values obtained from our simulations, that may also be obtained from a stability analysis of the 3D steady base flow prevailing after the first bifurcation. Indeed, when the primary instability is oscillatory, as happens in the case of a circular cylinder [1,13,27], the (nonlinear) frequency of the time-periodic limit cycle usually matches the (linear) frequency given by a global stability analysis close to criticality, whilst it does not necessary predict it as the Reynolds number increases far from Re_{co}. The same happens in the presence of a first stationary bifurcation and a secondary oscillatory mode when the perturbed base flow is considered in the linear stability analysis of the oscillatory bifurcation, as for the sphere wake [19,30,37]. Therefore, the authors believe that a more involved TriGLS analysis, employing the three-dimensional planar-symmetric base flow, would be valuable in order to predict with accuracy the linear stability properties close to the oscillatory neutral curve [31,32]. Such study would be complementary to our DNS because the methodology presented in our manuscript is able to capture the true bifurcations of the flow, as stated in Sect. 1.

3.1.3 Subsequent bifurcations

To conclude the incompressible study, we further explored the dynamics of the afterbody wake for the Reynolds numbers of 800, 900 and 1,000. As for other geometries as the sphere at Reynolds numbers larger than 325–360 [3,25] and a blunt-based axisymmetric body of length-to-diameter aspect ratio of 2 at $Re \sim 500$ [2], a low frequency develops in the present case when $Re \geq 800$. This phenomenon usually manifests through the modulation of the streamwise velocity perturbation [3,25,34], which is illustrated in Fig. 10c. According to [3], this event is not yet fully documented in the sphere wake and was (inaccurately) associated with the loss of the planar symmetry due to irregular variations in the azimuthal orientation of the vortex shedding [25,34]. The difficulty to reproduce experimentally the idealised theoretical scenario, which would allow us to observe the same solutions, was highlighted for a sphere rolling down an incline, which exhibits similar dual spectral peaks at $Re = 225$ and preserves the symmetry plane [28]. Planar symmetry is also preserved in the afterbody wake, at least, up to $Re = 900$, see Fig. 9b, even in the presence of the low frequency ($St_l = 0.0184$) which became dominant, see Fig. 10e, f. Bohorquez et al. [2] justified this finding in view of the developments of marked up oscillations upstream of the body base in the presence of vortex shedding, an effect that is more severe as the Reynolds number progressively increases. The current simulations corroborate that result. Interestingly, the ratio between the frequency of vortex shedding ($St^{3d}_{sat} = 0.118$) and the low frequency ($St_l = 0.023$) at inception ($Re = 800$), see Fig. 10d, is about 5 and differs from that of the sphere, i.e., 3–4 [25,34], and shorter

blunt-based axisymmetric bodies, i.e., 4 [2]. A possible explanation of such difference would be the different geometries employed in each study, because during this regime the wake interaction with the boundary layer on the solid surface is stronger than at lower Reynolds numbers [2]. The vortex shedding frequency slightly increased up to $\mathrm{St}_{\mathrm{sat}}^{3\mathrm{d}} = 0.137$ at $Re = 900$ and a new regime associated with the loss of the planar symmetry occurred in the range of Re between 900 and 1,000, as shown in Fig. 9c. Finally, one would expect a sharp increase of the dominant frequency in the range of $1{,}000 < Re < 4{,}140$ because of the development of turbulence, since the Strouhal number of the dominant frequency of the turbulent motion measured experimentally by Sevilla and Martínez-Bazán [26] increased asymptotically with the Reynolds number from 0.245 ($Re = 4140$) to 0.26 ($Re \approx 13000$). So the main frequency of the turbulent motion might not be related to the saturation frequency of the oscillatory motion $\mathrm{St}_{\mathrm{sat}}$, e.g., see Rodriguez et al. [23] for the turbulent flow over a sphere at $Re = 3{,}700$.

All the results reported here, complemented with those by Gumowski et al. [11], allow us to clarify the sequence of events that generate the different transitions in the laminar wake of an afterbody. Just below $Re_{\mathrm{cs}}^{3\mathrm{d}}$ the wake is axisymmetric and becomes unstable for $Re > Re_{\mathrm{cs}}^{3\mathrm{d}}$ when a pair of steady counter-rotating vortices develops. The intensity of the counter-rotating vortices increases with Re and the vortices elongate until $Re = Re_{\mathrm{co}}$, when they start oscillating without shedding vortices from the afterbody base. Such peristaltic instability exhibits many points in common with Crow instability in the presence of axial core flow: it is originated by a symmetric (S) mode and the vortices displace on planes inclined about 35° to the horizontal. By increasing even more the Reynolds number, we observe the increase of the oscillation amplitude and, subsequently, the peristaltic instability triggers the vortex shedding. The main difference of elongated bodies with respect to shorter geometries is that axial vorticity is less intense due to the shear forces on the surface that slow down the flow and changes the axial velocity profile at the body base. That might be the reason why the relative gap of the critical Reynolds numbers (Δ) is greater for longer bodies. Finally, when $Re > Re_{\mathrm{co}}$, the real flow is not only three-dimensional but also unsteady and might exhibit strong nonlinearities because of the excitation of non-linear frequencies in the wake (i.e. the low-frequency modulation and the harmonics of the main frequency) prior to the break of the planar symmetry.

3.2 Compressible regime, $M = 0.5$

In Sect. 3.1.1, we have shown the capabilities of DNS to compute and to describe the non-linear state of the perturbed base flow for $Re_{\mathrm{cs}} < Re < Re_{\mathrm{co}}$ in incompressible regime. Similarly, we present in Sect. 3.2.1 an exhaustive description of the perturbed base flow after the primary instability in compressible regime. We shall focus our attention on the subsonic speed $M = 0.5$ for which detailed BiGLS results are known [16,17]. Whilst both techniques are able to compute the critical value of Re_{cs}, the main advantage of DNS compare to the BiGLS is that it provides the full non-linear solution to the compressible Navier–Stokes equations instead of the linear perturbation equations. As a matter of fact, to the authors' knowledge the compressible planar-symmetric base flow has not been described beforehand for $Re_{\mathrm{cs}} < Re < Re_{\mathrm{co}}$ in the configuration under study here. Such results are essential to explain the evolution of Re_{co} with M and to better understand the oscillatory flow regimes at subsonic speed that we explore in Sect. 3.2.2.

So additional computations were performed for $M = 0.5$ to explore the effect of compressibility. In order to determine the flow regime, we followed the same procedure as for the incompressible analysis and, thus, the details of the methodology are not repeated herein.

3.2.1 Primary instability: loss of the flow axisymmetry

Firstly, we performed two numerical simulations at $Re = 470$ and 500 and found out a steady axisymmetric and planar-symmetric flow, respectively. This result establishes a lower bound and upper band for the critical Reynolds number of $Re_{\mathrm{cs}}^{3\mathrm{d}} = (470 + 500)/2 = 485$ with an error of $\pm 3\%$, see Fig. 3. Similar to the incompressible regime, these results agree with previous BiGLS that predicts the loss of the flow axisymmetry for $Re > Re_{\mathrm{cs}}^{\mathrm{GLS}} = 488.4$ (Table 1). The relative difference between $Re_{\mathrm{cs}}^{3\mathrm{d}}$ and $Re_{\mathrm{cs}}^{\mathrm{GLS}}$ is of $\pm 0.7\%$, showing that the accuracy of the current FVM is similar to FEM [16,17] not only in incompressible regime but also at subsonic speeds. Notice that the actual value of $Re_{\mathrm{cs}}^{\mathrm{GLS}} = 488.4$ (AR, private communication) slightly corrects the critical value of 483.5 reported in [16,17]. One could determine the exact value of $Re_{\mathrm{cs}}^{3\mathrm{d}}$ following the same procedure as described in Sect. 3.1, but the numerical simulations are very time consuming and, as we shall see below, there are no fundamental changes in the compressible planar-symmetric wake with respect to the incompressible one.

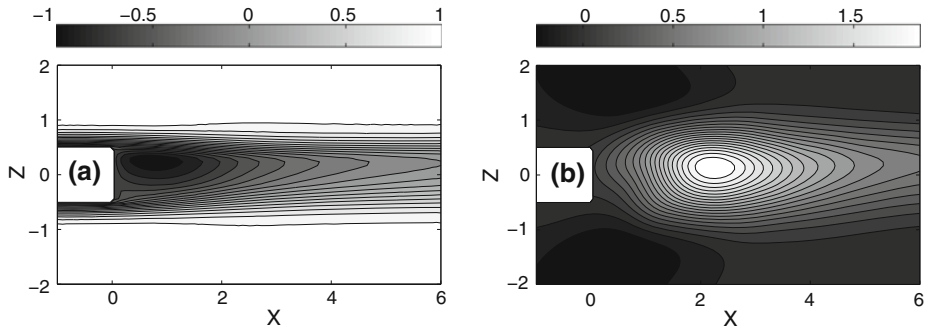

Fig. 12 **a** Streamwise velocity in the symmetry plane for $Re = 675$ and $M = 0.5$. **b** Difference ($\times 10^2$) between the incompressible ($M = 0$) and compressible ($M = 0.5$) streamwise velocity in the symmetry plane for $Re = 675$

Subsequently, we increased the Reynolds number up to 675 and the wake also reached a planar-symmetric steady state at late time. By inspecting the compressible velocity field, we observed that it was similar to the incompressible one. For the sake of the brevity, the contours of constant streamwise vorticity, which were nearly identical to those of the incompressible flow (see Fig. 4b), are not shown here. Instead, the dependence of the velocity field with the Mach number was quantified by computing the difference between the incompressible and compressible (Fig. 12a) streamwise velocity component, see Fig. 12b for the results obtained in the symmetry $\{x, z\}$-plane. As expected, the major discrepancy appeared close to the end of the (axisymmetric) recirculation bubble, of length $L_r \approx 2.2$ at $Re = 675$ and $M = 0.5$, though there were no qualitative differences. Therefore, compressibility does not alter the structure of the planar-symmetric velocity field.

One aspect that is highlighted regards the identification of the differences between the density and temperature fields of the planar-symmetric perturbed flow with respect to the axisymmetric base flow for $Re = 675$ and $M = 0.5$. Recall that the symmetry plane is the $\{x, z\}$-plane. Figure 13a depicts the density field of the axisymmetric background flow, whilst Fig. 13b, c show, respectively, contours of the perturbed density field in the $\{x, y\}$- and $\{x, z\}$-plane. The shape of the axisymmetric and perturbed field in the $\{x, y\}$-plane were found similar and the differences were, interestingly, lower that 0.5% (see Fig. 14a), even in the presence of swirl in the perturbed flow. The double tail composed by a counter-rotating vortex pair also induced a misalignment of the density field with respect to the streamwise direction, as observed in Fig. 13c, but the relative differences in the $\{x, z\}$-plane were as small as in the $\{x, y\}$-plane, see Fig. 14b. It is worth mentioning that the density variation of the perturbed flow with respect to the axisymmetric base flow progressively decreased upstream of the afterbody base and was lower than 0.05%. Furthermore, the azimuthal density variations in the planar-symmetric flow vanished upstream of the solid base, which is in accordance with vanishing magnitudes of perturbation predicted by BiGLS [16]. Hence, we believe that the global instability originated near the afterbody base hardly affects the density field close to the afterbody nose, at least for the present afterbody aspect ratio. Finally, the temperature behaved as the density, and the maximum relative difference with respect to the unperturbed flow shown in Fig. 14c, d, i.e. 0.15%, was even lower than for the density.

3.2.2 Secondary and subsequent bifurcations

We increased the Reynolds number from 675 to 700 for $M = 0.5$. In order to avoid reporting transient effects, we proceeded as for incompressible flows. By examining the temporal evolution of the three velocity components during the numerical simulation, we ran the case during a minimum of ten cycles of the lowest frequency. We obtained at late time a monochromatic signal for the streamwise velocity component of constant amplitude and with the Strouhal number of $\mathrm{St}_{\mathrm{sat}}^{\mathrm{3d}} = 0.109$, which is associated with periodic shedding of vortices, see Fig. 15a. At this Reynolds number, vortices were shed from the afterbody base, indicating that the flow is supercritical. Given the proximity between the upper bound ($Re = 700$) and lower band ($Re = 675$) for the shedding of vortices, we did not perform numerical simulations at intermediate values of the Reynolds number. Instead, we estimated the critical value as the average of $Re_{\mathrm{co}}^{\mathrm{3d}} = 687.5$, which is represented in Fig. 3 together with the error bar of $\pm 1.85\%$. Notice the similarity between the incompressible and compressible vorticity contours shown in Figs. 9a and 15a, respectively. In accordance with the finding by Xin et al. [37] in the wake flow around a sphere, no fundamental changes were observed in the compressible regime justifying our exhaustive incompressible study in Sect. 3.1. Indeed, the axisymmetric BiGLS analysis [16,17] also predicted a small variation of the compressible critical parameters, $\mathrm{St}_{\mathrm{sat}}^{\mathrm{GLS}} = 0.063$ and $Re_{\mathrm{co}}^{\mathrm{GLS}} = 998.5$ (see Fig. 3), though

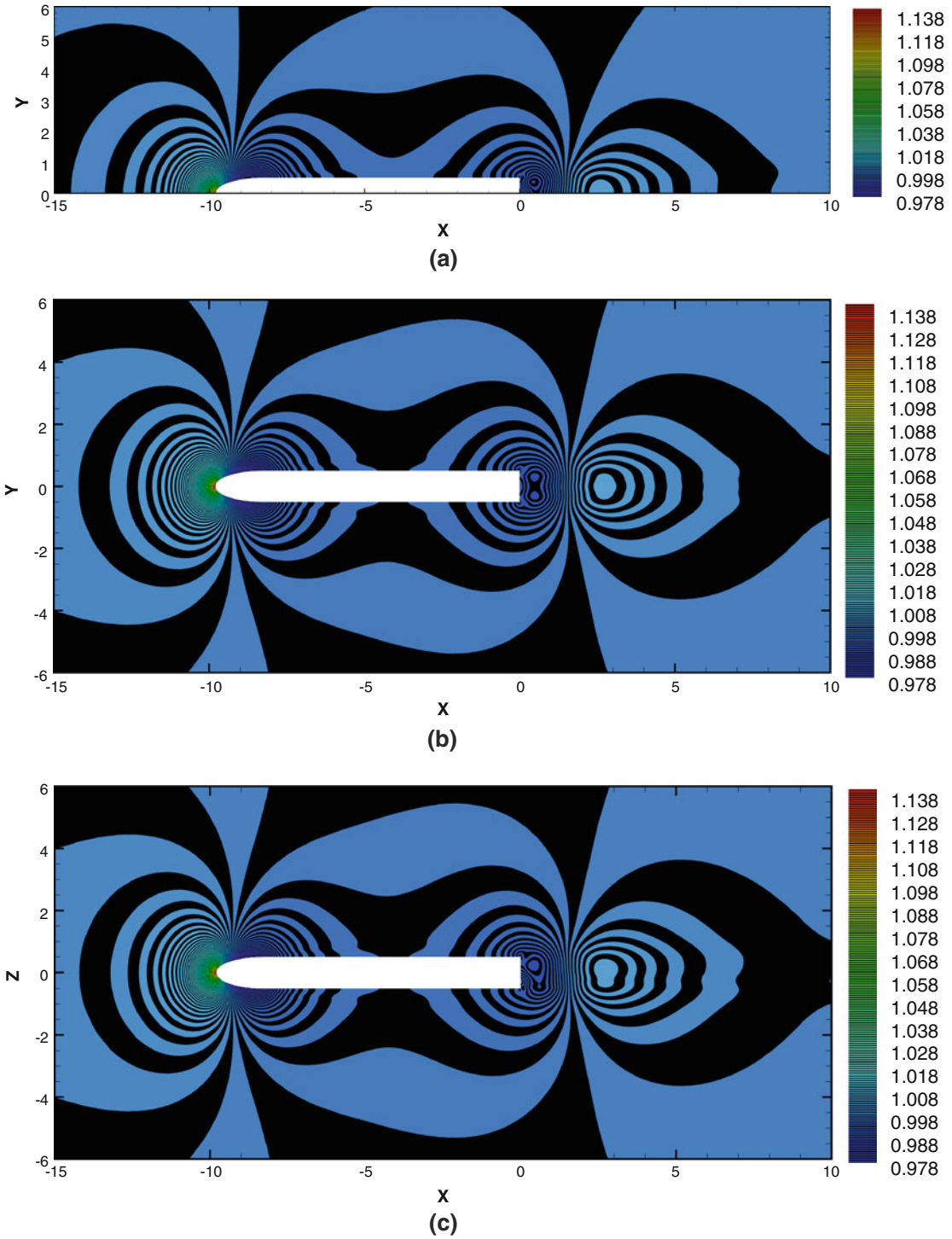

Fig. 13 Contours of constant density, ρ, for $Re = 675$ and $M = 0.5$: **a** axisymmetric background flow, **b**, **c** steady planar-symmetric perturbed flow in the $\{x, y\}$ and $\{x, z\}$ plane, respectively. Each level differs in 5×10^{-4}

they remain far from the DNS values. The low increment in the true value of $Re_{\mathrm{co}}^{\mathrm{3d}}$ with M can be understood in part because of the small variations of the steady, planar-symmetric velocity field described for the first time in Sect. 3.2.1. As a matter of fact, we reported a relative difference between the compressible ($M = 0.5$) and incompressible ($M = 0$) planar-symmetric velocity field lower than 1.5% close to criticality ($Re = 675$). Such differences would be even lower for $M < 0.5$ because compressible effects decrease with Mach number.

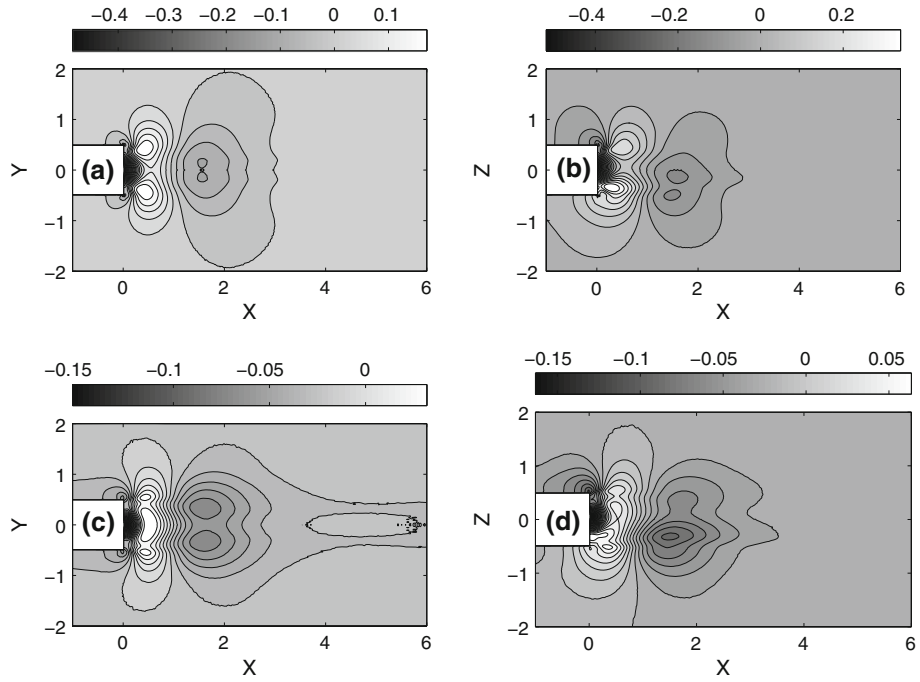

Fig. 14 Relative difference (%) of the axisymmetric density (**a**, **b**) and temperature (**c**, **d**) fields with respect to the three-dimensional perturbed flow for $Re = 675$ and $M = 0.5$

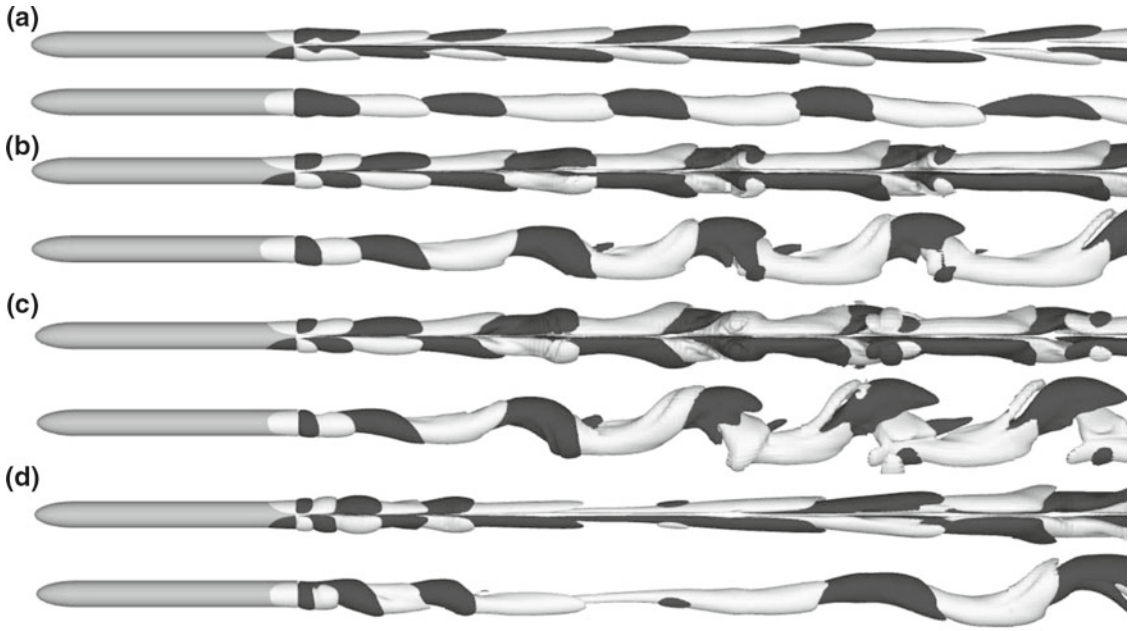

Fig. 15 Contours of constant streamwise vorticity, $\omega_x = \pm 0.05$, at $M = 0.5$ for $Re = 700$ (**a**), 800 (**b**), 900 (**c**) and 1,000 (**d**). Plan view is rotated 90° with respect to the lateral view

The slow variation of Re_{co} also indicates that the dominant three-dimensional mode is nearly independent of the Mach number for $M \leq 0.5$, and that the secondary instability is unrelated to effects of compressibility. Similar results were found for three-dimensional instabilities in compressible flow over open cavities by Brès and Colonius [4]. Subsequently, the discrepancy between $Re_{\mathrm{co}}^{\mathrm{3d}}$ and $Re_{\mathrm{co}}^{\mathrm{GLS}}$ is to be attributed to the break of the axisymmetry of the flow past the first regular bifurcation, as for incompressible flows.

In addition, we explored the flow regimes at the higher Reynolds numbers of $Re = 800$, 900 and 1,000. Figure 15 shows the contours of constant streamwise vorticity at late time for each case, illustrating that the planar-symmetric state is preserved, at least, up to $Re = 1{,}000$. The aspect of the vorticity contours at $Re = 800$

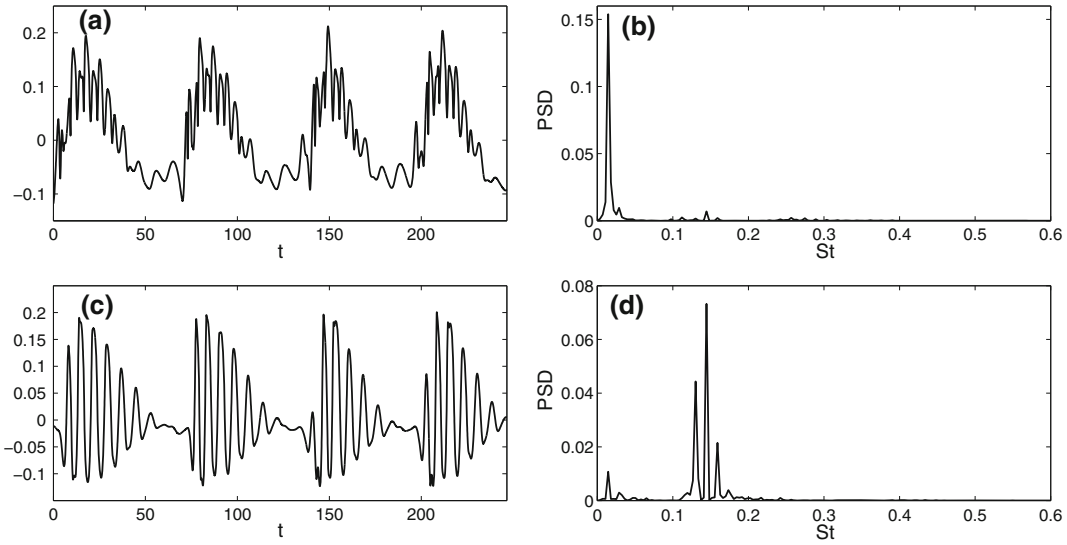

Fig. 16 Time history (*left column*) and PSD (*right column*) of the velocity fluctuations [2] for $M = 0.5$ and $Re = 1{,}000$: **a**, **b** streamwise velocity component; **c**, **d** tangential velocity component. The nondimensional value of t in the abscissa of **a** and **c** was reinitialized to show just the saturated periodic state ($t > 0$). Probes were sampled at ($x = 3$, $y = 0$, $z = 0$)

(Fig. 15b) and 900 (Fig. 15c) is quite similar to that of incompressible flow at the same Reynolds numbers, e.g. see Fig. 9b for $Re = 900$. By inspecting the PSD of the streamwise velocity component at $Re = 800$, we observed the developments of the harmonics of the main frequency $\mathrm{St}_{\mathrm{sat}}^{3\mathrm{d}} = 0.117$ and a low-frequency modulation corresponding to $\mathrm{St}_{\mathrm{l}} = 0.0173$, as for incompressible flow (recall Fig. 10c, d). So the ratio between the main and low frequency is of 6.75 at $Re = 800$ and $M = 0.5$. Such value is larger than that of 5 corresponding to the same Reynolds number in incompressible regime, see Sect. 3.1.3. On the other hand, the excitation of new frequencies in the wake (i.e. the low-frequency modulation and the harmonics of the main frequency) leads to a decrease of the energy associated with the leading velocity fluctuations due to the non-linear energy transfer from the natural frequency $\mathrm{St}_{\mathrm{sat}}$ to the newly excited ones. Indeed, the increment of the energy associated with the low-frequency modulation is much more evident at $Re = 1{,}000$. Figure 16a depicts the details of the streamwise velocity oscillations for $Re = 1{,}000$ at ($x = 3$, $y = 0$, $z = 0$), whilst the associated PSD is shown in Fig. 16b. As happens for supercritical, incompressible flows far enough from criticality, the dominant frequency of the motion along the x-axis, $\mathrm{St}_{\mathrm{l}} = 0.0144$, is much lower than the vortex shedding frequency ($\mathrm{St}_{\mathrm{sat}}^{3\mathrm{d}}$). The dominance of the low frequency manifests as the shed of weaker vortices or thinner filaments, approximately, every 60 time units, as shown in Fig. 15d. In the PSD of the streamwise velocity fluctuations is difficult to identify $\mathrm{St}_{\mathrm{sat}}^{3\mathrm{d}}$ and, consequently, we followed our previous work [2] where we analysed the oscillations of the tangential velocity component, see Fig. 16c, d, which yields $\mathrm{St}_{\mathrm{sat}}^{3\mathrm{d}} = 0.144$. Such values lie very close to the incompressible ones of $\mathrm{St}_{\mathrm{sat}}^{3\mathrm{d}} = 0.143$ and $\mathrm{St}_{\mathrm{l}} = 0.0145$ for the same Reynolds number. Interestingly, the ratio between the frequency of vortex shedding and the low frequency is, approximately, of 10 at $Re = 1{,}000$ both at subsonic speeds and for incompressible flow. In doing so for lower Reynolds numbers, we found that the vortex shedding frequency varies, approximately, as $\mathrm{St}_{\mathrm{sat}}^{3\mathrm{d}}(Re) = 0.00012\,(Re - Re_{\mathrm{co}}^{3\mathrm{d}}) + 0.1058$.

So we found out that compressibility effects delay the loss of the planar symmetry of the wake reported in incompressible regime between $Re = 900$ and 1,000, see Sect. 3.1.3. This is the most noticeable difference we found between incompressible ($M = 0$) and compressible ($M = 0.5$) flows up to the Reynolds numbers of $Re = 1{,}000$. Notice that even in the absence of the loss of the planar symmetry, we have reported the developments of low frequencies that are from 5 to 10 times lower than the saturation frequency of the oscillatory motion. In the widest studied case of spheres shaped geometries, the low frequency was incorrectly associated with the break of the planar symmetry of the flow [2] and our study reports now that there is no connection between the developments of the low frequency St_{l} and the loss of the planar symmetry, not only in incompressible regime but also at subsonic speeds.

According to our results, the flow at $M = 0.5$ and $Re > 700$ is not only three-dimensional but also unsteady and might exhibit strong nonlinearities as for the incompressible regime. Indeed, our DNS indicates that at $M = 0.5$ and $Re = 1{,}000$ the real flow is three-dimensional and highly unsteady because of the excitation of non-linear frequencies in the wake (i.e. the low-frequency modulation and the harmonics of the main frequency). However, Meliga et al. [17] evaluated the sensitivity of BiGLS eigenvalues to forcing at $M = 0.5$

and $Re = 998.5$ ($\approx$1,000) considering a steady, axisymmetric base flow. Linear stability might not work well so far from the true value of $Re_{co} \approx 687.5$ and hence we expect a strong impact of base flow nonlinearities on the linear sensitivity analysis carried out in [17]. Consequently, results in [17] on the control of the oscillatory global mode of the afterbody at $M = 0.5$ and $Re = 998.5$, although are interesting from a theoretical point of view, are questionable in terms of applicability and deserve further research.

4 Conclusions

In this article, we have performed direct numerical simulations of the wake flow of an afterbody at low Reynolds number ($Re \leq 1{,}000$) in the incompressible ($M = 0$) and compressible ($M = 0.5$) regimes. We have shown that the bifurcation scenario is not fundamentally changed with respect to the incompressible flow behind a sphere. With increasing Reynolds number, the initially stable and axisymmetric base flow undergoes a first stationary bifurcation at $Re_{\rm cs} \approx 463$ ($M = 0$) and $Re_{\rm cs} \approx 485$ ($M = 0.5$) owing the loss of the flow axisymmetry. The current numerical simulations accurately predict the first instability and are in excellent agreement with previous known axisymmetric biglobal linear stability analysis, see Fig. 3. We have found that the intensity of the azimuthal velocity monotonously increases with the Reynolds number, which induces a misalignment with the symmetry plane: the higher the Reynolds grows, the larger the eccentricity observed (see Figs. 2, 4). Subsequently, we have reported the transition to a periodic state at $Re_{\rm co} \approx 678.2$ ($M = 0$) and $Re_{\rm co} \approx 687.5$ ($M = 0.5$). For incompressible flows, we have shown that the secondary bifurcation corresponds with a three-dimensional peristaltic oscillation, modulating the two parallel counter-rotating vortices, as shown in Fig. 5b and supplementary videos 1–4. To the authors' knowledge, this second instability has not been documented in the wake flow of an afterbody beforehand. It has been shown that this modulation of the vortices is closely related to Crow instability in the presence of axial core flow: it is originated by a long-wavelength symmetric mode, the vortex centres displace on planes inclined about 35° to the horizontal, see Fig. 8, and the scaled nondimensional wavelength λ/b decreases from about 20 ($x = 0$) to 8 ($x = 60$) whilst the nondimensional wavelength λ takes the constant value of 8. The ensuing bifurcation scenario is not fundamentally changed with respect to previous axisymmetric biglobal linear stability predictions, though both the critical Reynolds number for the onset of oscillation, $Re_{\rm co}$ (see Fig. 3), and the Strouhal number of the time-periodic limit cycle, $\mathrm{St}_{\rm sat}$ (see Sect. 3), are substantially shifted in comparison with the sphere case. Interestingly, though the sequence of bifurcations is analogous to that found in the wake flow around a sphere, e.g. [11], our gap between critical Reynolds numbers is higher, 0.4 versus 0.27, and the axisymmetric biglobal linear stability does not work well because it neglects the primary bifurcation and the real, planar-symmetric base flow diverges from the fictitious axisymmetric solution at $Re > Re_{\rm cs}$. No fundamental changes are observed in the compressible regime. Subsequently, in order to quantify the stability properties of the pair of trailing vortices with axial core flow close to the oscillatory neutral curve for the geometry under consideration, we highlight the need of triglobal linear stability analysis [19,30,31,37] complementary to our DNS. Furthermore, for incompressible and compressible flows in the range of $800 \leq Re \leq 1{,}000$, we have reported the excitation of new frequencies in the wake (i.e. the low-frequency modulation and the harmonics of the main frequency) which leads to a decrease of the energy associated with the leading velocity fluctuations. The developments of the low-frequency modulation at $Re \approx 800$ are clearly not associated with the loss of the planar symmetry of the wake, which occurs at $M = 0$ in the range of Re between 900 and 1,000. Furthermore, the loss of the planar symmetry did not occur at $M = 0.5$ in such interval of Reynolds numbers. The values of the low frequency are from 5 to 10 times lower than the saturation frequency of the oscillatory motion $\mathrm{St}_{\rm sat}$ for the parameter values studied here. Subsequently, we expect a strong impact of base flow nonlinearities on the linear sensitivity analysis carried out in reference [17] for $M = 0.5$ and $Re = 998.5$, and so our findings have important consequences not only for the oscillatory critical parameters but also for the control of the oscillatory global mode. We conclude by pointing out that several of our findings are not fully documented for the wake flow behind a sphere, and thus, the results reported herein may serve to motivate a more involved stability analysis [19,30,31,37].

Acknowledgments This work has been partially supported by the Spanish MCyT (projects # DPI2008-06624-C02 and ICTS-2009-40), Junta de Andalucía (project # P07-TEP02693) and European funds. The computer time was provided by the Centro de Supercomputación de Galicia (CESGA) under project number ICTS-CESGA 142 and by the Centro Informatico Científico de Andalucía (CICA). The authors are also grateful to the anonymous reviewers and the editorial team for their constructive remarks, which were essential in revising the paper.

References

1. Barkley, D.: Linear analysis of the cylinder wake mean flow. Europhys. Lett. **75**(5), 750–756 (2006)
2. Bohorquez, P., Sanmiguel-Rojas, E., Sevilla, A., Jiménez-González, J., Martínez-Bazán, C.: Stability and dynamics of the laminar wake past a slender blunt-based axisymmetric body. J. Fluid Mech. **676**, 110–144 (2011)
3. Bouchet, G., Mebarek, M., Dušek, J.: Hydrodynamic forces acting on a rigid fixed sphere in early transition regimes. Eur. J. Mech. B/Fluids **25**, 321–336 (2006)
4. Brès, G.A., Colonius, T.: Three-dimensional instabilities in compressible flow over open cavities. J. Fluid. Mech. **599**, 309–339 (2008)
5. Brion, V., Sipp, D., Jacquin, L.: Optimal amplification of the Crow instability. Phys. Fluids **19**, 111703 (2007)
6. Colonius, T.: Modeling artificial boundary conditions for compressible flow. Annu. Rev. Fluid Mech. **36**, 315–345 (2004)
7. Crow, S.: Stability theory for a pair of trailing vortices. AIAA J. **8**(12), 2173–2179 (1970)
8. Ferziger, J.H., Perić, M.: Computational Methods for Fluid Dynamics. Springer, Berlin (2002)
9. Ghidersa, B., Dušek, J.: Breaking of axisymmetry and onset of unsteadiness in the wake of a sphere. J. Fluid Mech. **423**, 33–69 (2000)
10. Greenshields, C.J., Weller, H.G., Gasparini, L., Reese, J.M.: Implementation of semi-discrete, non-staggered central schemes in a colocated, polyhedral, finite volume framework, for high-speed viscous flows. Int. J. Numer. Meth. Fluids **63**(1), 1–21 (2010)
11. Gumowski, K., Miedzik, J., Goujon-Durand, S., Jenffer, P., Wesfreid, J.E.: Transition to a time-dependent state of fluid flow in the wake of a sphere. Phys. Rev. E **77**(5), 055308 (2008)
12. Johnson, T.A., Patel, V.C.: Flow past a sphere up to a Reynolds number of 300. J. Fluid Mech. **378**, 19–70 (1999)
13. Leontini, J.S., Thompson, M.C., Hourigan, K.: A numerical study of global frequency selection in the time-mean wake of a circular cylinder. J. Fluid. Mech. **645**, 435–446 (2010)
14. Leweke, T., Williamson, C.: Experiments on long-wavelength instability and reconnection of a vortex pair. Phys. Fluids **23**, 024101 (2011)
15. Meliga, P.: A theoretical approach for the onset and control of unsteadiness in compressible afterbody flows. Ph.D. thesis, École Polytechnique (2008)
16. Meliga, P., Sipp, D., Chomaz, J.M.: Effect of compressibility on the global stability of axisymmetric wake flows. J. Fluid Mech. **660**, 499–526 (2010)
17. Meliga, P., Sipp, D., Chomaz, J.M.: Open-loop control of compressible afterbody flows using adjoint methods. Phys. Fluids **22**, 054109 (2010)
18. Moore, D., Saffman, P.: The instability of a straight vortex filament in a strain field. Proc. R. Soc. Lond. A **346**, 413–425 (1975)
19. Morzyński, M., Thiele, F.: Finite element method for global stability analysis of 3D flows. In: 4th AIAA Flow Control Conference, art. no. 2008-3865 (2008)
20. Natarajan, R., Acrivos, A.: The instability of the steady flow past spheres and disks. J. Fluid Mech. **254**, 323–344 (1993)
21. Ormières, D., Provansal, M.: Transition to turbulence in the wake of a sphere. Phys. Rev. Lett. **83**(1), 80–83 (1999)
22. Pier, B.: Local and global instabilities in the wake of a sphere. J. Fluid Mech. **603**, 39–61 (2008)
23. Rodriguez, I., Borrell, R., Lehmkuhl, O., Perez-Segarra, C.D., Oliva, A.: Direct numerical simulation of the flow over a sphere at Re = 3700. J. Fluid Mech. **679**, 263–287 (2011)
24. Roy, C., Leweke, T., Thompson, M., Hourigan, K.: Experiments on the elliptic instability in vortex pairs with axial core flow. J. Fluid Mech. **677**, 383–416 (2011)
25. Schouveiler, L., Provansal, M.: Self-sustained oscillations in the wake of a sphere. Phys. Fluids **14**(11), 3846–3854 (2002)
26. Sevilla, A., Martínez-Bazán, C.: Vortex shedding in high Reynolds number axisymmetric bluff-body wakes: Local linear instability and global bleed control. Phys. Fluids **16**, 3460–3469 (2004)
27. Sipp, D., Lebedev, A.: Global stability of base and mean flows: a general approach and its applications to cylinder and open cavity flows. J. Fluid. Mech. **593**, 333–358 (2007)
28. Stewart, B.E., Thompson, M.C., Leweke, T., Hourigan, K.: Numerical and experimental studies of the rolling sphere wake. J. Fluid Mech. **643**, 137–162 (2010)
29. Storti, M.A., Nigro, N.M., Paz, R.R., Dalcín, L.D.: Dynamic boundary conditions in computational fluid dynamics. Comput. Methods Appl. Mech. Eng. **197**, 1219–1232 (2008)
30. Tezuka, A., Suzuki, K.: Three-dimensional global linear stability analysis of flow around a spheroid. AIAA J. **44**(8), 1697–1708 (2006)
31. Theofilis, V.: Global linear instability. Annu. Rev. Fluid Mech. **43**, 319–352 (2011)
32. Theofilis, V., Colonius, T.: Special issue on global flow instability and control. Theor. Comput. Fluid Dyn. **25**(1–4), 1–6 (2011)
33. Thompson, M., Leweke, T., Provansal, M.: Kinematics and dynamics of sphere wake transition. J. Fluids Struct. **15**, 575–585 (2001)
34. Tomboulides, A.G., Orzsag, S.A.: Numerical investigation of transitional and weak turbulent flow past a sphere. J. Fluid Mech. **416**, 45–73 (2000)
35. Tsai, C.Y., Widnall, S.E.: Stability of short waves on a straight vortex filament in a weak externally imposed strain field. J. Fluid Mech. **73**, 721–733 (1976)
36. Viswanath, P.R.: Flow management techniques for base and afterbody drag reduction. Prog. Aerospace Sci. **32**, 79–129 (1996)
37. Xin, X., Liu, Y., Ma, D., Sun, D.: Three-dimensional global linear stability analysis of compressible flow around a sphere. Chin. J. Comput. Phys. **28**(1), 10–18 (2011)